SUPPLEMENTAL FIGURES

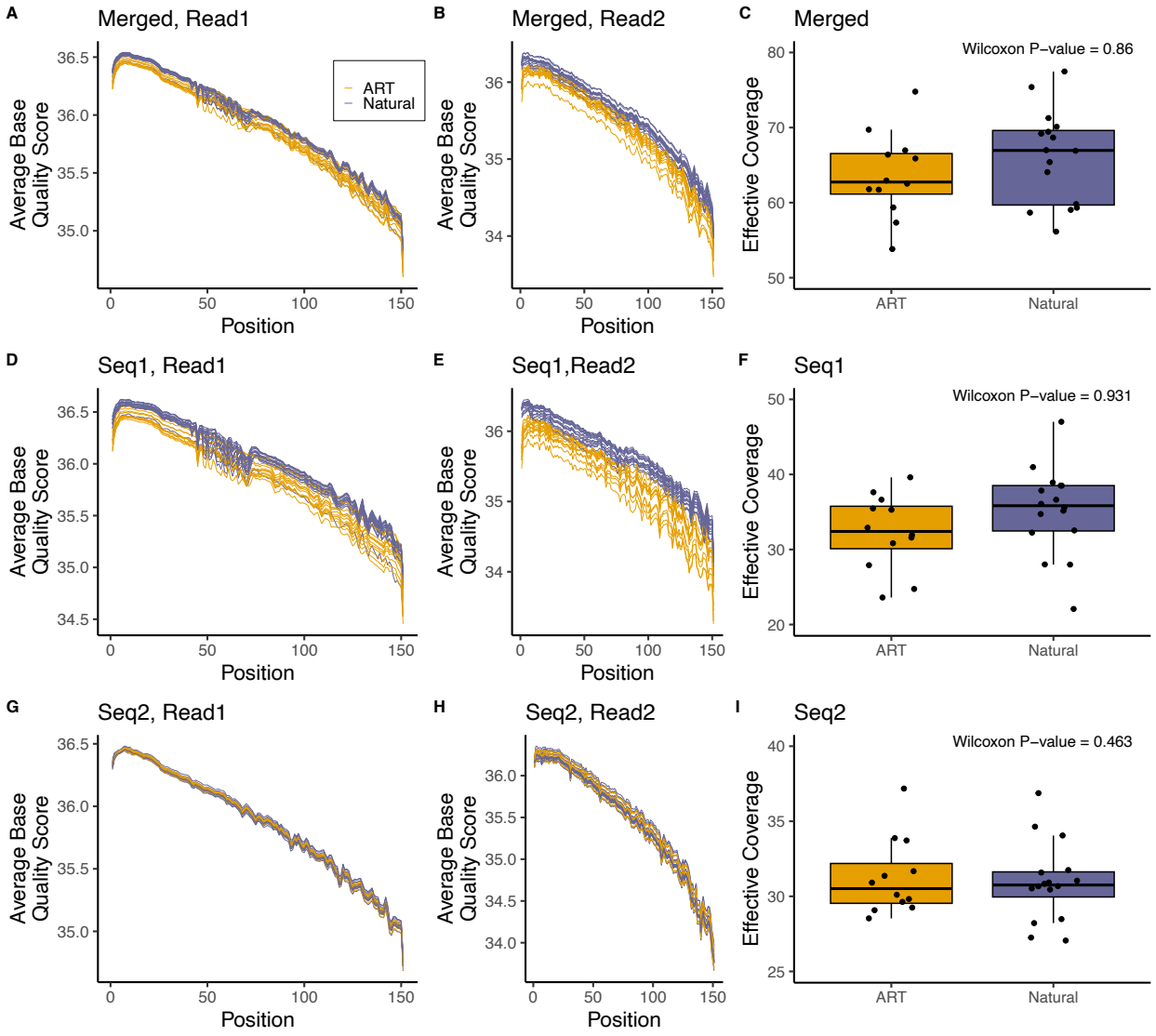

Supplemental Figure 1. *Base quality scores by read position and sequencing coverage for ART- (orange) and natural-born samples (purple). Two replicate paired-end 150 bp libraries were prepared from each sample and sequenced in two batches, referred to as Seq1 and Seq2. Average base quality scores across each base position in Read1 in the merged data (A) and both individual sequencing libraries (D, G). Average base quality scores across each base position in Read2 in the merged data (B) and individual Seq1 (E) and Seq2 (H) libraries. High-quality sequencing reads were obtained from both breeding cohorts in both sequencing batches, although reads from ART-derived samples have slightly lower base quality scores compared to natural-born samples in the Seq1 sequencing batch. Effective sequencing coverage for the merged, Seq1, and Seq2 data (C, F, I). Coverage estimates exclude duplicated reads and assume a genome size of 2.7Gb. Samples from both ART- and natural-born cohorts were sequenced to identical target coverage in both Seq1 and Seq2. However, a batch effect in sample preparation, library construction, and sequencing manifested as a higher rate of duplicated reads in the ART-derived samples compared to natural-born samples during Seq1 data collection (F).*

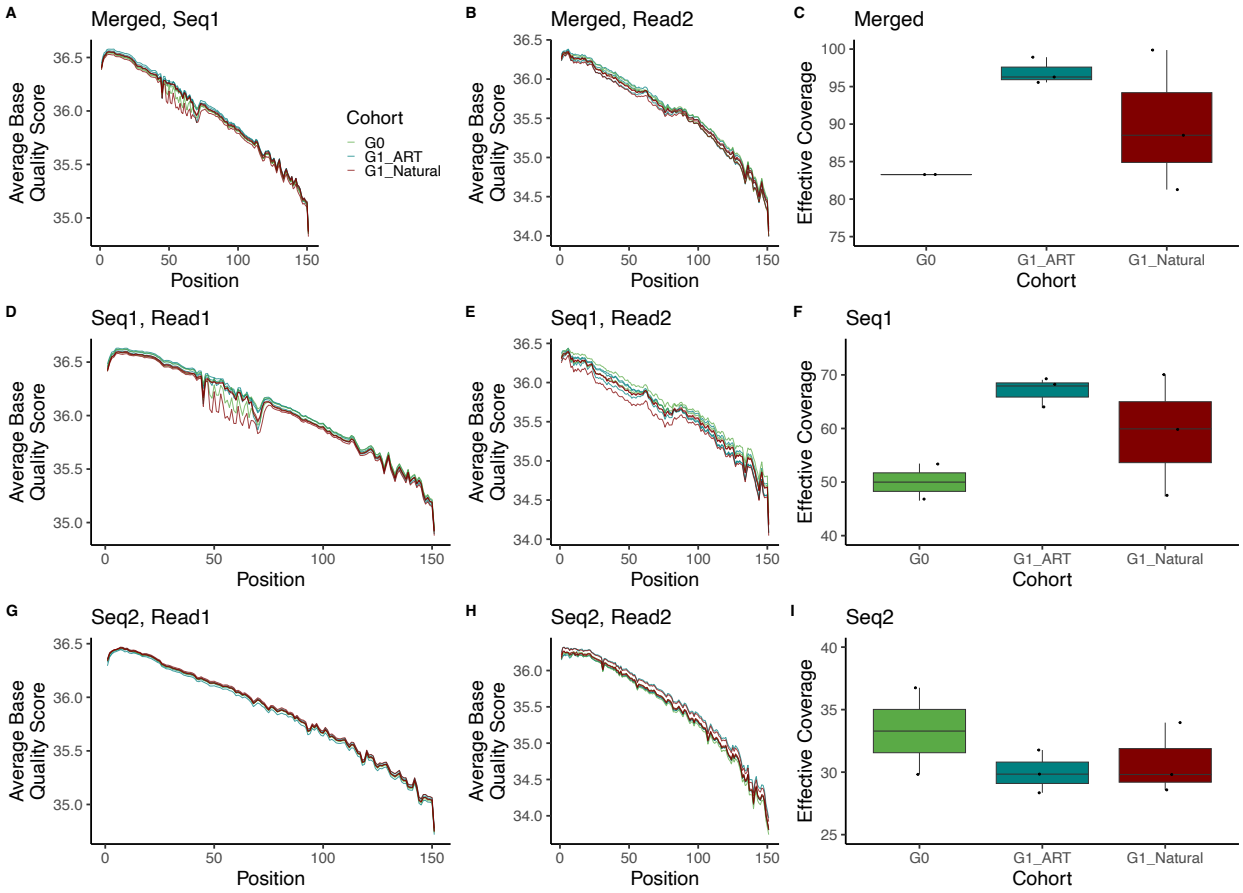

Supplemental Figure 2. *Base quality scores by read position and sequencing coverage for the G0 pedigree founder pair and G1 parents of the ART- and natural-born G2 cohorts. Two libraries were prepared from each sample and processed in two different sequencing runs, Seq1 and Seq2. Average base quality scores across each base position in Read1 for the merged sequencing data (A) and individual Seq1 (D) and Seq2 (G) sequencing data. Average base quality scores across each base position in Read2 for the merged, Seq1, and Seq2 sequencing data (B, E, H). Effective sequencing coverage for the merged, Seq1, and Seq2 sequencing data (C, F, I).*

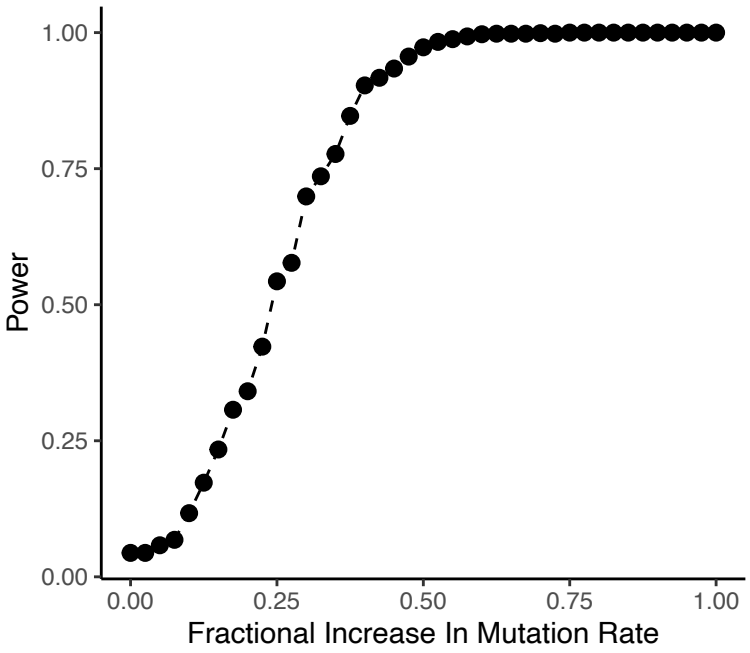

Supplemental Figure 3. *Power to detect mutation rate differences under the analyzed experimental conditions. We simulated dnSNVs in each G2 sample according to a Poisson distribution, with rate parameter set to the number of expected germline mutations (genome size × mutation rate in per base/per generation units). Simulations assume an average callable genome size of 2.23 Gb, a baseline mutation rate of 0.5 x 10^{-8} per base per generation, and impose read depth requirements of ≥10 total reads and ≥3 reads per allele. Binomial sampling was used to capture the uncertainty associated with transmission of mutations arising in the G1 germline to the G2 generation. The mutation rate of the simulated natural cohort was held at the simulated baseline rate, whereas the mutation rate of the simulated ART cohort was increased by a fixed proportion across simulation sets (x-axis). The difference in mutation tallies among the simulated natural and ART cohorts was assessed by a negative binomial generalized linear mixed model of the form: dnSNV count ~ Cohort. We performed a total of 1000 simulation replicates for each fractional increase in mutation rate in the ART cohort, retaining the cohort term P-value from each replicate. Power was computed as the fraction of simulated datasets for which P < 0.05. R code to reproduce simulations and this figure is available as supplemental material.*

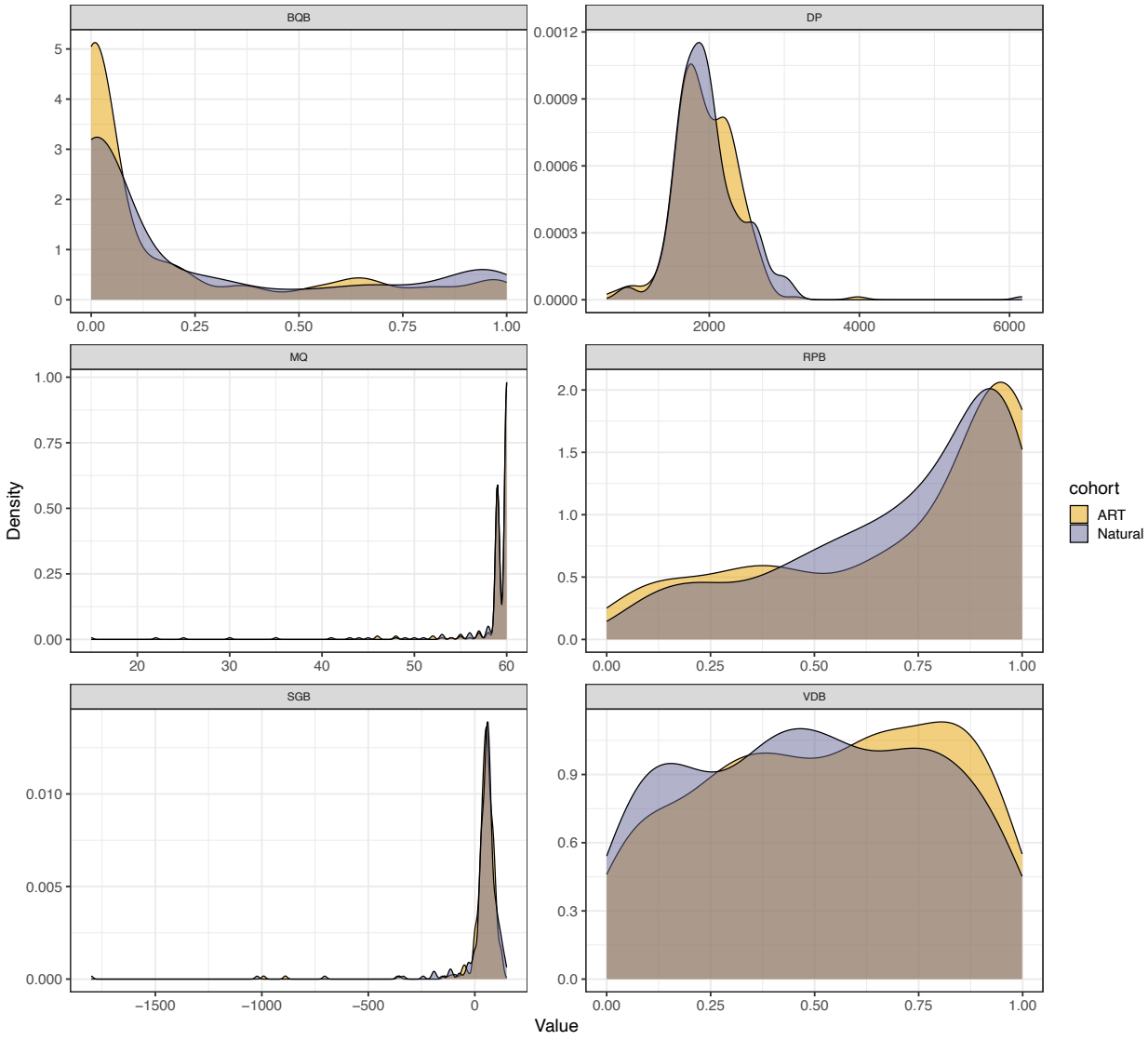

Supplemental Figure 4. *Distribution of Mpileup variant annotations for dnSNVs in ART-(yellow) and naturally-conceived (purple) progeny. Annotations include: Base Quality Bias (BQB), Depth of Coverage (DP), Mapping Quality (MQ), Read Position Bias (RPB), Segregation-Based Score (SGB), and Variant Distance Bias (VDB). Distributions for each annotation metric are identical between the two groups (Kolmogorov-Smirnov Test, P > 0.05).*

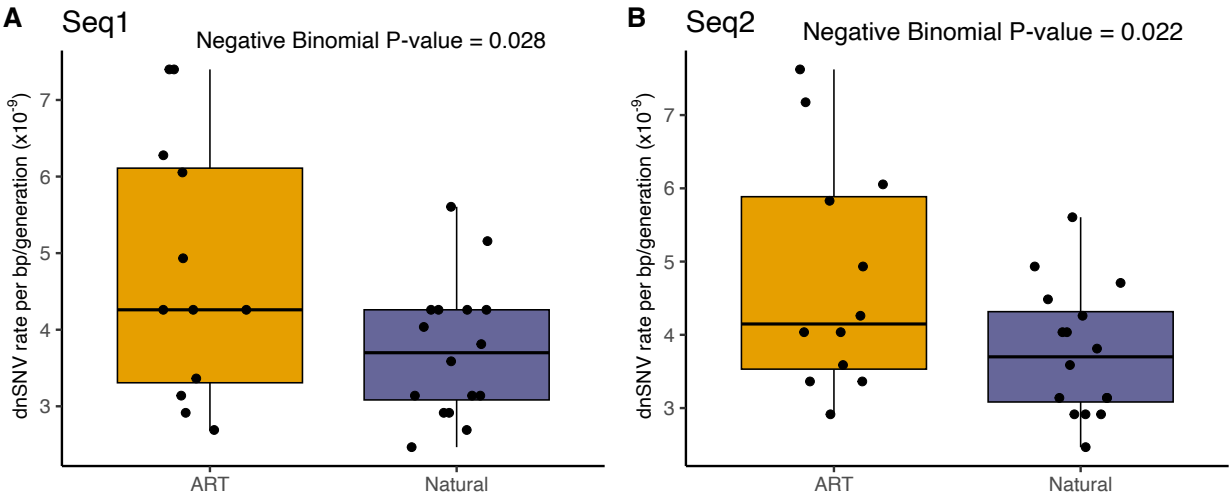

Supplemental Figure 5. *Boxplots showing the median, interquartile range, and full range of dnSNV rates per bp/generation across G2 samples. dnSNV calls were derived using only sequencing data from (A) Seq1 and (B) Seq2.*

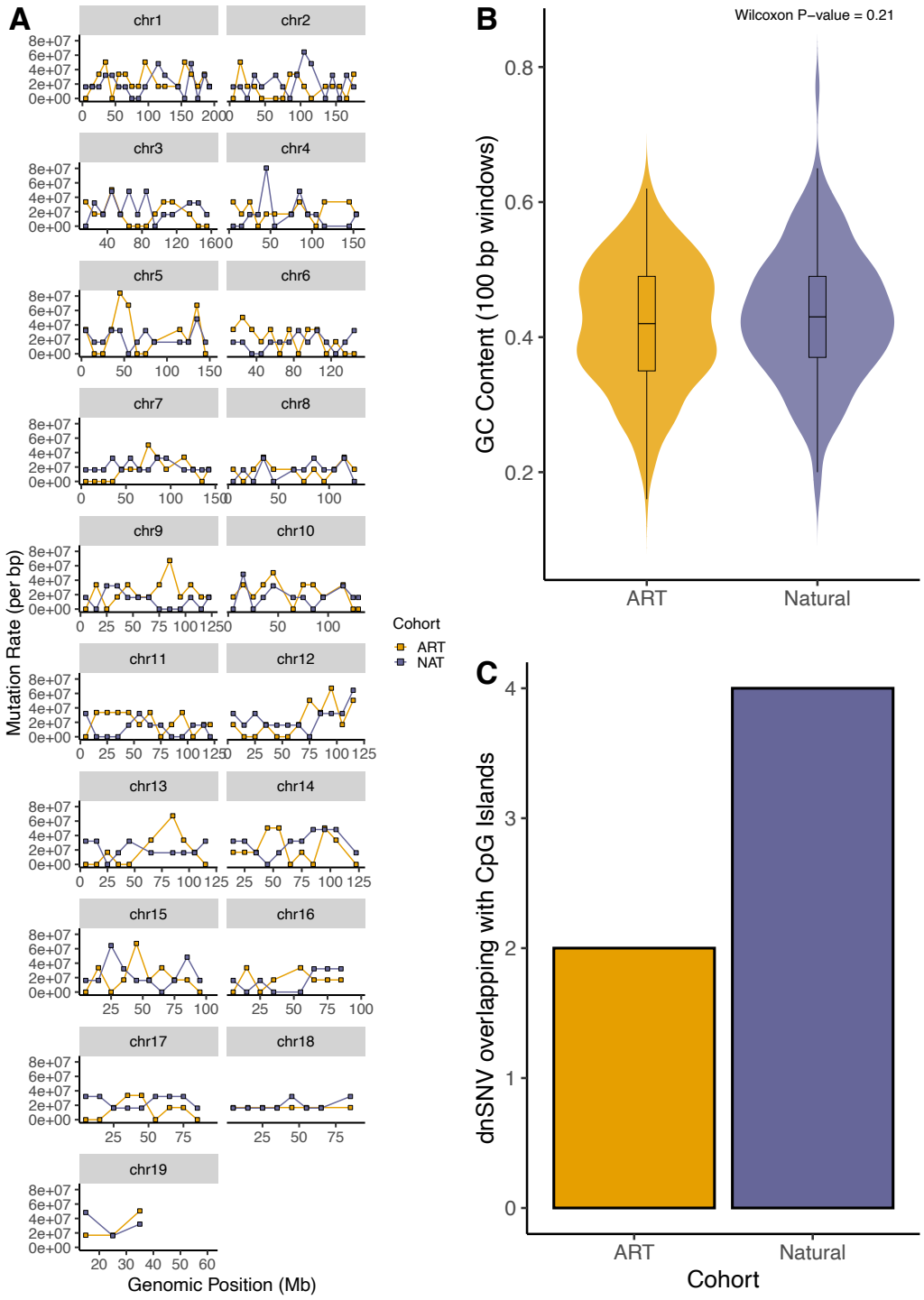

Supplemental Figure 6. *(A) Genomic distribution of dnSNVs in ART-derived (orange) and natural-born (purple) cohorts. Mutation counts were aggregated in 10 Mb windows across the autosomal genome. (B) Violin plots depicting the distribution of GC content in 100 bp windows centered on dnSNVs identified in both cohorts. Embedded boxplots represent the interquartile range and median GC content. (C) Bar plot showing the percentage of dnSNVs in ART-and natural-born samples that overlap CpG islands. There is no cohort-level difference (Fisher's exact test, P = 0.6862).*

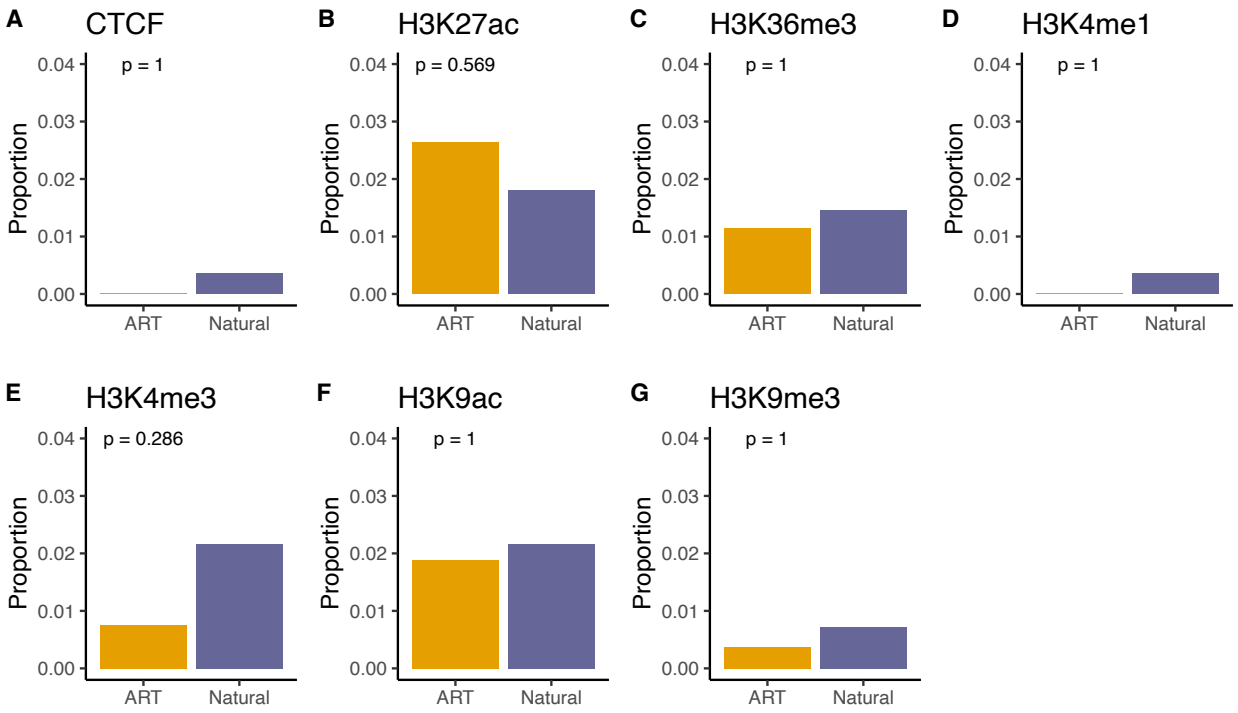

Supplemental Figure 7. *Proportion of dnSNVs in ART- and naturally-born samples that overlap ChIP-seq peaks associated with (A) CTCF binding or (B-G) various histone modifications in mESCs. P-values were computed from Fisher's exact tests. ChIP-seq data are from the Bruce4ES dataset released with the Mouse ENCODEproject (Stamatoyannopoulos et al. 2012).*

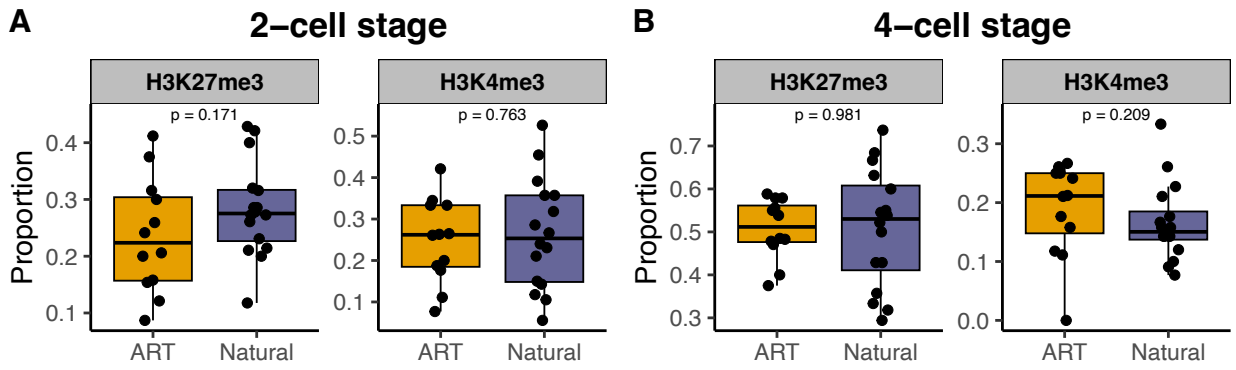

Supplemental Figure 8. *Proportion of dnSNVs in ART- and naturally-born samples that overlap H3K27me3 and H3K4me3 ChIP-seq peaks in 2-cell stage (A) and 4-cell stage (B) mouse embryos. ChIP-seq data are from a published source (Liu et al. 2016). Significance was assessed by a two-tail Wilcoxon rank-sum test.*

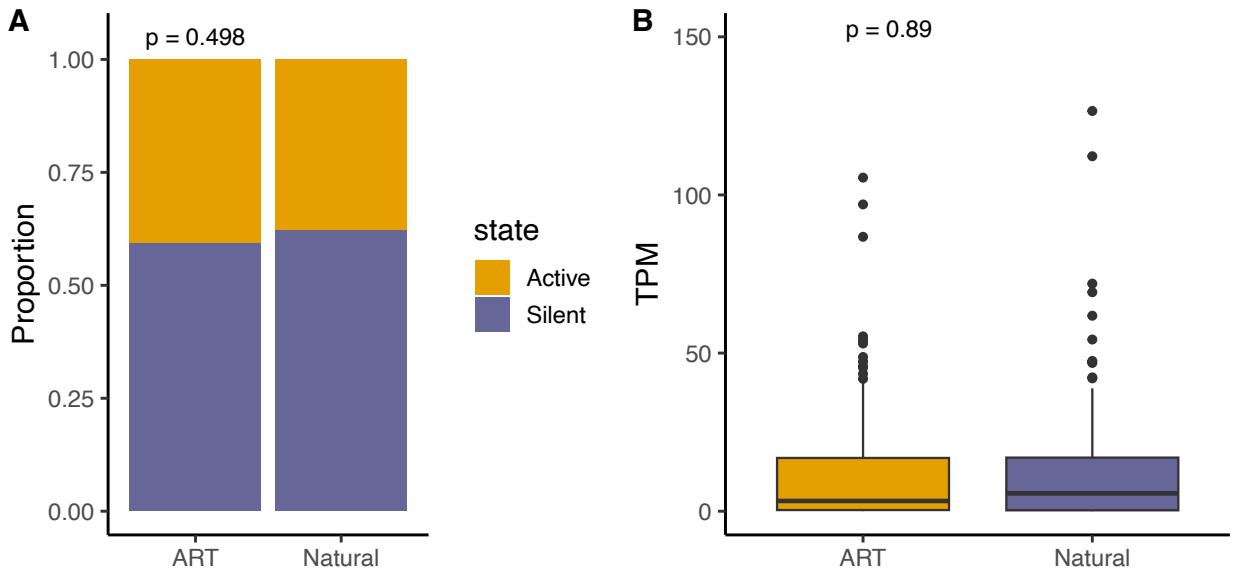

Supplemental Figure 9. *No difference in dnSNV distribution between ART- and natural-born progeny with respect to the transcriptional activity of neighboring genes in C57BL/6J mouse ESCs. dnSNVs were intersected with neighboring genes, with a 2.5kb allowance upstream of the gene start and downstream of the gene end. Both (A) the proportion of dnSNVs near genes that are expressed (Active) versus silenced (Silent) and (B) the overall transcript abundance of active genes expressed as transcripts per million (TPM) are indistinguishable between cohorts. Significance was assessed by a Fisher's exact test (A) or Wilcoxon rank-sum test (B).*

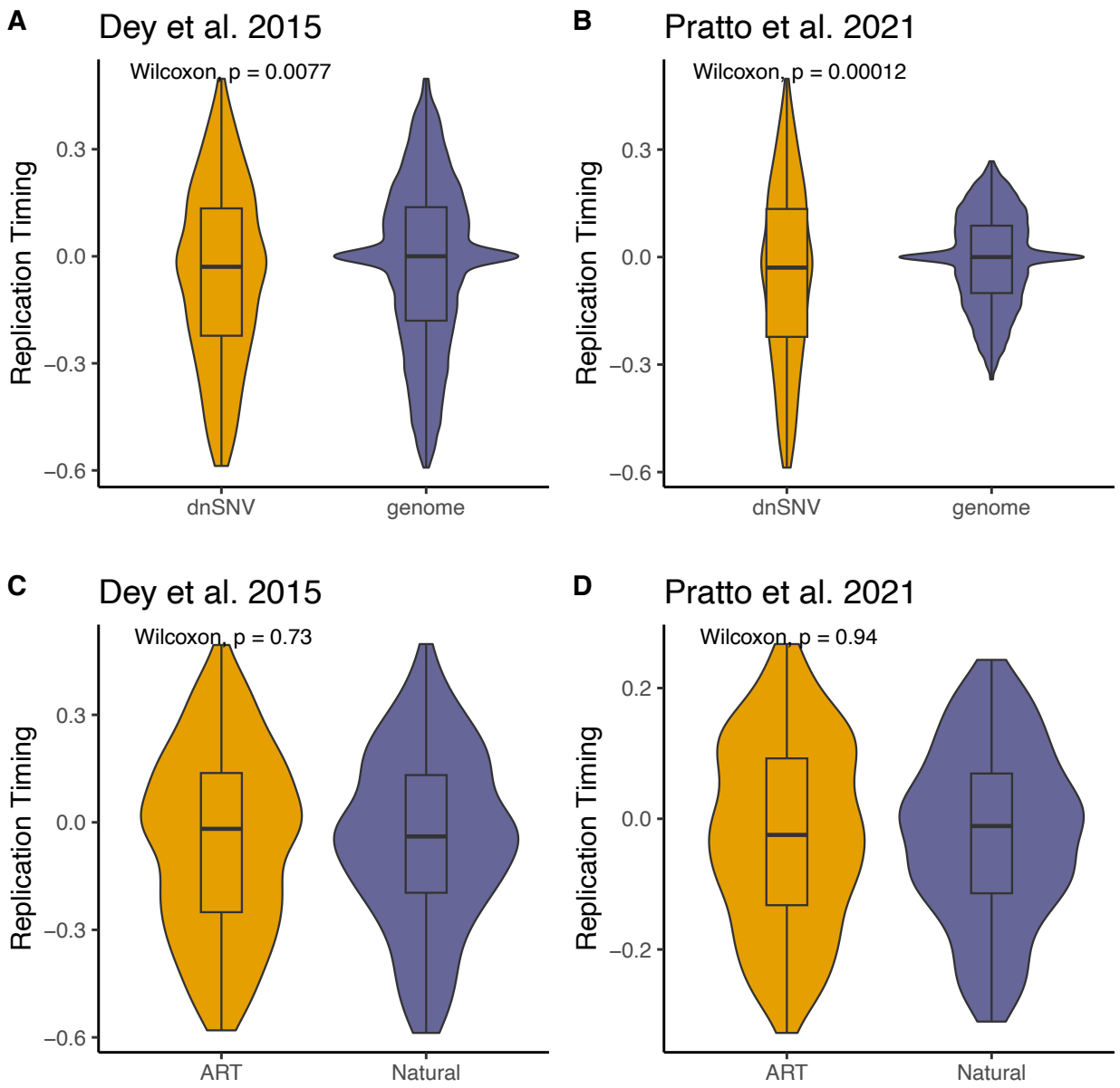

Supplemental Figure 10. *Replication timing at dnSNVs. Replication timing estimates were based on published Repli-seq datasets for mESCs* (Dey et al. 2015; Pratto et al. 2021) *and plotted as violin plots with inset boxplots indicating median (thick black line) and interquartile range (box height). Replication timing estimates are presented as log2 early/late ratios, with lower values indicating regions that replicate later and more positive values consistent with earlier replication. Differences in replication timing between tested groups were evaluated using two-tailed Wilcoxon rank-sum tests. (A and B) Replication timing comparisons between aggregate dnSNVs discovered in both ART and natural-born mouse cohorts compared to genome-wide distribution of replication timing. dnSNVs are enriched in late replicating regions. (C and D) No difference in replication timing of dnSNVs in ART- versus natural-born mice.*

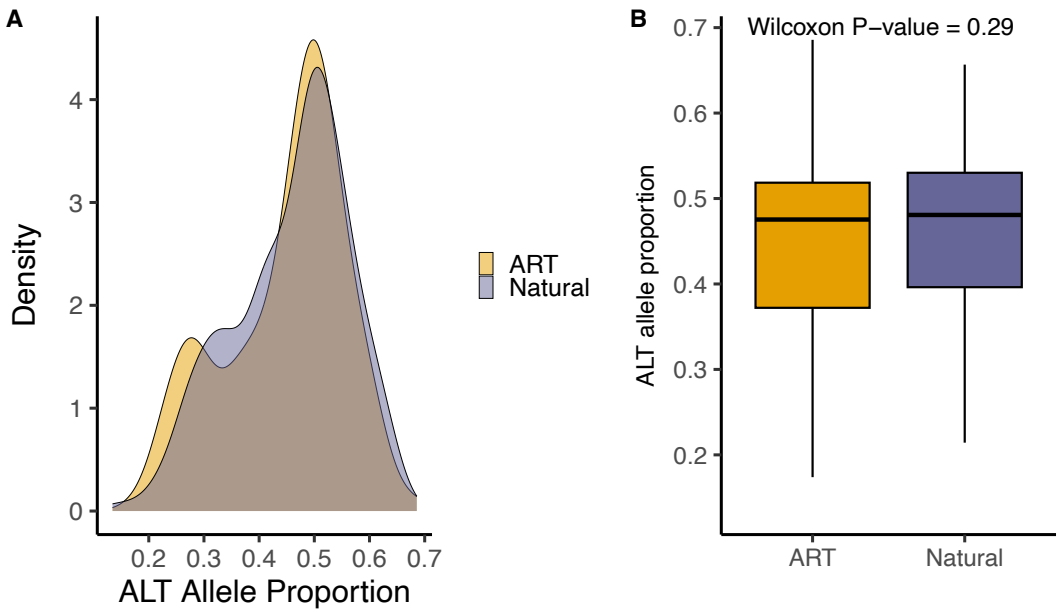

Supplemental Figure 11: *Distribution of ALT allele proportion by cohort. (A) Density plot showing the distribution of ALT allele proportions for dnSNVs in each cohort. (B) Boxplot comparing ALT allele proportions between cohorts.*